Chitosan-miRNA Functionalized Microporous Titanium Oxide Surface via A Layer-by-layer Approach with a Sustained Release Profile for Enhanced Osteogenic Activity

Kaimin Wu
Navy 971st Hospital
Mengyuan Liu
Qingdao Municipal Hospital Group
Nan Li
Navy 971st Hospital
Li Zhang
Fourth Military Medical University
Fanhui Meng
Fourth Military Medical University
Lingzhou Zhao (zhaolingzhou1983@hotmail.com)
Fourth Military Medical University
Min Liu
Navy 971st Hospital
Yumei Zhang
Fourth Military Medical University

Research

Keywords: microRNAs, sustained release, layer-by-layer, microarc oxidation, mesenchymal stem cells, titanium implants

Posted Date: May 19th, 2020

DOI: https://doi.org/10.21203/rs.3.rs-29493/v1

Version of Record: A version of this preprint was published on September 9th, 2020. See the published version at https://doi.org/10.1186/s12951-020-00674-7.

Abstract

Background: Biofunctionalization of titanium implants for high osteogenic ability holds the hope for advanced implant of promoted osseointegration, especially in the compromised bone condition. In this study, using chitosan-miRNA (CS-miRNA) complex and sodium hyaluronate (HA) as the positively and negatively charged polyelectrolyte, the polyelectrolyte multilayers (PEMs) were fabricated using the layer-by-layer approach on the microarc oxidized (MAO) Ti surface via silane glutaraldehyde coupling.

Methods: Dynamic contact angle and scanning electron microscopy were firstly analyzed to monitor the layer accumulation. RiboGreen was used to quantify the miRNA loading and release profile in phosphate-buffered saline. *In vitro* transfection efficiency and cytotoxicity were investigated after mesenchymal stem cells (MSCs) being seeded on the CS-antimiR-138/HA PEM functionalized microporous Ti surface. The *in vitro* osteogenic differentiation of MSCs and *in vivo* osseointegration were also inspected.

Results: The surface wettability alternately changed during the formation of PEMs. The CS-miRNA nanoparticles distributed evenly along the MAO surface. The miRNA loading amount increased with the bilayer number increasing. More importantly, a sustained miRNA release of over approximately 2 week was obtained. *In vitro* transfection revealed that the CS-antimiR-138 nanoparticles were taken up efficiently by the cells and caused significant knockdown of miR-138 without showing significant cytotoxicity. The CS-antimiR-138/HA PEM surface enhanced osteogenic differentiation of MSCs on it in terms of enhanced alkaline phosphatase, collagen product and extracellular matrix mineralization. In the rat model, it led to dramatically enhanced *in vivo* osseointegration.

Conclusions: All these findings demonstrate that novel CS-antimiR-138/HA PEM functionalized microporous Ti implant exhibits sustained release of CS-antimiR-138, and obviously enhances the *in vitro* osteogenic differentiation of MSCs and dramatically enhanced *in vivo* osseointegration. This novel miRNA functionalized Ti implant may be used in clinic to allow more effective and robust osseointegration.

Introduction

Titanium (Ti) implants are widely applied as orthopedic and dental implants. Though high success has been achieved, increasing clinical requirement for faster and tighter osseointegration calls for further improvement [1, 2]. Conventional implant modification techniques such as alteration of surface properties (eg. suitable micro, submicro and nanoscale topographies and wettability [3–6]) and loading and delivery of inorganic elements [7, 8] are suggested to have limited effect in osteogenic activity enhancement [9]. Biofunctionalization of Ti implant with more potent biochemical cues, such as extracellular matrix (ECM) proteins [10], peptides [11, 12], growth factors [13, 14] as well as nucleotides [15, 16], shall give rise to more predictable osseointegration, especially in compromised bone condition.

MicroRNAs (miRNAs) are endogenous small non-coding RNAs of 19–25 nucleotides in size, which play important roles in a variety of diverse and fundamental biological processes, such as cell development,

proliferation, differentiation, apoptosis and signal transduction. It is believed that miRNAs mimic the natural differentiation pathway and give a delicate control of multiple genes constituting a much healthier stimulator of stem cell differentiation [17]. Recently, the reports on the regulating effect of miRNAs on osteogenesis keep expanding [18–21], among which miR–138 is reported to be a negative regulator of the osteogenic differentiation of mesenchymal stem cells (MSCs). AntimiR–138 inhibiting the endogenous miR–138 level is reported to enhance the bone formation *in vivo.*[18] In our previous proof-of-concept studies, antimiR–138 lipoplexes have been introduced to the cell culture plate and the Ti surface to enhance the osteogenic differentiation of MSCs cultured on them [22]. Before possible clinical application, it is important to use a more biocompatible carrier instead of liposomes as well as control the loading and delivering kinetics of antimiR–138 to achieve a sustainable effect.

As a natural degradable cationic polymer, chitosan (CS) showing good stability and cytocompatibility has already been used for the delivery of DNA and RNA [23–26]. Via electrostatic interaction, CS can bind miRNAs to form relatively stable CS-miRNA nanoplexes (NPs) with positive charge. We know that positively and negatively charged polyelectrolytes can be alternately adsorbed via electrostatic adsorption, called the layer-by-layer (LbL) technology, to fabricate the polyelectrolyte multilayer (PEM) film [27, 28]. PEM with controlled loading and release profile has been experimentally used to deliver growth factors [29, 30], DNA molecules [31, 32], RNA molecules [33, 34], etc. Here it is proposed that CS-antimiR–138 NPs and hyaluronic acid (HA, a commonly used polyanion in LbL) can be used to PEM-functionalize the Ti bone implant for sustainable antimiR–138 delivery and consequently augmented osseointegration.

Two important issues for developing the CS-antimiR–138/HA PEM functionalized microporous Ti implant are stable immobilization of the first monolayer to the Ti surface and loading amount enhancement. The amine groups in CS can covalently bond to the hydroxyl groups via simple silane-glutaraldehyde coupling. Hence, chemical pretreatment of Ti with (3-aminopropyl) triethoxy silane (APTES) and glutaraldehyde (GA) has been widely used for a stable CS coating [35–37]. Interestingly, the facile and economical microarc oxidation (MAO) treatment of Ti followed by ultraviolet (UV) irradiation can result in increased hydroxyl groups on the Ti implant surface, further favoring the silane-glutaraldehyde coupling [38]. Meanwhile, the MAO microporous Ti surface shall possess improved loading capacity. In this study, the CS-antimiR–138/HA PEM-functionalized MAO-Ti implant was developed by LbL and silane-glutaraldehyde coupling, whose *in vitro* and *in vivo* performance was studied (Scheme 1).

Materials And Methods

Materials

Commercially pure Ti discs (15 mm in diameter and 2 mm in thickness) and screw Ti rods (2.8 mm in diameter and 6 mm in length) were provided by the Northwest Institute for Nonferrous Metal Research, Xi’an, China. CS (molecular weight 100 kDa and deacetylation degree of 95%) was purchased from Jinke

Co. Ltd. (China). β-glycerophosphate disodium salt pentahydrate, calcium acetate momohydrate, APTES, GA, ascorbic acid, dexamethasone, Sirius Red, Alizarin Red and dimethyl sulfoxide (DMSO) were purchased from Sigma-Aldrich Company (USA). Solution RNase Erasol was bought from TIANDZ (China). α-minimal essential medium (α-MEM), fetal bovine serum (FBS), penicillin and streptomycin were obtained from Hyclone (USA). Cell count kit–8 (CCK–8), lactate dehydrogenase (LDH), 3,39-dioctadecyloxacarbocyanineperchlorate (DiO) and BCIP/NBT Alkaline Phosphatase Color Development Kit were provided by Beyotime (China). Phosphate buffered saline (PBS), 4',6-diamidino–2-phenylindole (DAPI) were purchased from Invitrogen (USA). E. Z. N. A.^{TM} Total RNA Kit I was obtained from OMEGA (USA). PrimeScriptTM RT reagent kit and SYBR Premix ExTM Taq II were purchased from TaKaRa (Japan). Male SD rats (6–8 weeks old) were obtained from the laboratory animal center of the Fourth Military Medical University. The antimiR–138 (CGGCCUGAUUCACAACACCAGCU) and negative control (CAGUACUUUUGUGUAGUACAA) were synthesized from Shanghai Gene Pharma Co., Ltd (China).

Fabrication of the CS-antimiR–138/HA PEM functionalized microporous Ti through LbL

Pure Ti discs were polished with waterproof abrasive paper from 400 to 1500 grids and then ultrasonically cleaned in acetone, ethanol and distilled water for 10 min each. The Ti discs were then treated in the electrolyte containing β-glycerophosphate disodium salt pentahydrate (0.02 M) and calcium acetate monohydrate (0.2 M) at 400 V DC for 5 min. After ultrasonic cleaning and drying, the fabricated MAO Ti samples were sterilized for 30 min by UV irradiation.

CS and HA were dissolved in 0.2 M sodium acetate buffer (pH = 5.5) and deionized water (pH = 5.5), respectively, at the concentration of 1 mg/ml. Both CS and HA were sterilized using a 0.22 μm syringe filter and then treated with Solution RNase Erasol Kit according to the manufacturer's instruction. Afterwards, 100 μl antimiR–138 (20 mM in RNA-free water) was added into 1 ml final CS solution quickly followed by magnetic stirring for 10 min and incubation for 30 min at room temperature. The N/P ratio (the molar ratio of chitosan amino groups to RNA phosphate groups) in our experiment was 60, calculated with a mass per phosphate of 325 Da for RNA and mass per charge of 163 Da for chitosan (95% deacetylation). The CS-antimiR–138 NPs were then observed using a transmission electron microscope (TEM, JEM–1200EX, JEOL Ltd., Japan).

The CS-antimiR–138/HA PEM coating was then fabricated on MAO Ti via LbL. The dried MAO Ti discs were immersed in a 10 % (v/v) solution of APTES in alcohol in sealed individual containers for 2 h on the shaker. Then the MAO discs were placed in pure alcohol and sonicated for 30 min, which was repeated twice more for a total sonication time of 90 min. Afterwards, the Ti discs were rinsed with deionized water twice to remove residual alcohol and then dried. To link GA to the MAO-APTES surface, the GA solution (2.5 (v/v) in deionized water) was poured over the MAO-APTES samples ensuring complete coverage of the metal coupon. The containers were then sealed for 1 h. Afterwards, the samples were rinsed thoroughly with deionized water for 3 times. The CS dissolved in 0.2 M sodium acetate buffer (10 mg/ml,

pH 5.5) was poured over the Ti surface for 20 min. After washing with sodium acetate buffer, the Ti sample was then alternatively dipped into the HA solution and CS-antimiR–138 solution for 10 min each. Every dipping step was followed by two washings with sodium acetate buffer to remove excess materials. The steps were repeated until a desired number of bilayers was obtained.

Characterization of the CS-antimiR–138/HA PEM functionalized microporous Ti

The surface morphology of the prepared Ti samples was observed by field-emission scanning electron microscope (FE-SEM, Hitachi S–4800). In order to assess the miRNA loading, Cy3-labeled miRNAs (Gene Pharma) were used to fabricate the coating. Immediately after fabrication or after 7 days of incubation in α-MEM supplemented with 10% FBS, the Ti samples were observed by a laser scanning confocal microscope layer by layer with an interlayer thickness of 400 nm (Fluo View, Olympus FV1000). The three-dimensional images were reconstructed.

Quantification of the loading and release of miRNA from the CS-antimiR–138/HA PEM functionalized microporous Ti

To measure the miRNA loading amount in each layer of the functionalized surface, 40 μl CS-miRNA nanoparticles were dropped discreetly in the experiment and incubated for 10 min. Then the coated surface was washed twice by 40 μl sodium acetate buffer. Afterwards, the washing solution was carefully collected and quantitatively analyzed by RiboGreen assay according to the manufacturer's instruction. Finally, the miRNA loading amount in each layer was calculated by subtracting the miRNA amount in the washing solution from that of the original 40 μl CS-miRNA nanoparticles. The total miRNA loading amount in the PEM was calculated by adding the amount in each layer up.

The CS-antimiR–138/HA PEM functionalized microporous Ti samples were incubated in 300 μl PBS (pH = 7.4) at 37 °C in 5% CO_2 and 100% humidity for 14 days. At 8, 16, and 24 h, and 2, 3, 4, 6, 8, 10, 12 and 14 days, the extracting solution was replaced with 300 μl of fresh PBS solution. The released miRNA in the collected PBS solution was quantified with RiboGreen assay. As a reference, a standard curve for miRNA concentration was determined with multiple dilution of miRNA in PBS and PBS alone.

Cell culture

Primary rat bone marrow MSCs were obtained from two-week-old Sprague-Dawley rats. The cells were cultured in α-MEM supplemented with 10% FBS and 1% penicillin/streptomycin and incubated in a humidified atmosphere of 5% CO_2 at 37 °C. Passages 2–4 were used in this experiments. The MAO surface and tissue culture plate served as control. The medium was replaced twice every week.

Transfection efficiency assay

Here the functionalized Ti samples made of Cy3-labeled miRNAs were used. MSCs of $2.5\times10^4/cm^2$ were inoculated on the Ti samples placed in the 24 well plates. After 48 h of culture, the transfected cells were harvested by trypsin, washed with PBS and fixed in 1% paraformaldehyde. To clearly observe the internalization of the Cy3-labeled miRNAs to the cells, the cells were fixed with 4% paraformaldehyde and washed in PBS. The cell membrane was stained with DiO. The cell nucleus was highlighted with DAPI. The DiO, DAPI and Cy3 fluorescence signals were then observed by the laser scanning confocal microscope. To measure the miR–138 amount in the cells, RNA in the cells was collected and reverse-transcribed using a PrimeScript RT reagent kit and a specific reverse transcription primer (Shanghai Gene Pharma Co, Ltd) according to the manufacturer's recommendation. The miR–138 amount was quantified using a real-time polymerase chain reaction (Real-time PCR) system (CFX96™, Bio-Rad, Hercules, CA, USA) with SYBR Premix Ex Taq™ II. U6 small nuclear RNA was used as an endogenous normalization control.

Cell viability and Lactate dehydrogenase activity assay

The CCK–8 assay was employed to evaluate the cell viability according to the manufacturer's instruction. Briefly, the reaction medium was formed by mixing serum free α-MEM and CCK–8 at a ratio of nine to one. MSCs of $2.5\times10^4/cm^2$ were inoculated on the Ti samples placed in the 24 well plates. After 24 h of culture, the medium was removed and the Ti samples were washed with PBS twice. Then 400 μl reaction medium was added to each well and incubated at 37 °C for 3 h. The supernatant was transferred to a 96-well plate and the optical density (OD) was determined using a spectrophotometer (Bio-tek) at 450 nm wavelength.

The LDH activity in the culture medium was used as an index of cytotoxicity. After 24 h of culture, the culture medium was collected and centrifuged, and the supernatant was used for the LDH activity assay. The LDH activity was determined spectrophotometrically according to the manufacturer's instruction.

Cell morphology

MSCs were seeded at a density of 5×10^4 cells/well. After 24 h of culture, the Ti samples with attached cells were gently washed with PBS, fixed in 2.5% glutaraldehyde, dehydrated in a graded ethanol series and freeze-dried. After sputter coating with carbon, the cell morphology was observed by FE-SEM.

In vitro osteogenesis of MSCs

The expression of osteogenisis-related genes was evaluated using the Real-time PCR. The cells were seeded with 5×10^4 cells/well and cultured for 48 h. Then the medium was changed into osteogenic

medium containing 10 mM β-glycerophosphate, 50 μg/ml ascorbic acid and 10^{-7} M dexamethasone. After further culture of 7 and 14 days, the total RNA was isolated using the TRIzol reagent. Then 2 μg RNA from each sample was reversed transcribed into complementary DNA (cDNA) using the PrimeScript RT reagent kit. The expression of osteogenesis-related genes including collagen type I α1 (COL1), runt-related transcription factor 2 (RUNX2), alkaline phosphatase (ALP), bone morphogenetic protein–2 (BMP–2), osterix (OSX) and osteocalcin (OCN) was quantified using Real-time PCR. The PCR reaction was carried out using SYBR Premix Ex Taq™ II on the CFX96™ Real-time PCR System. The relative expression levels for each gene of interest were normalized to that of the housekeeping gene GAPDH. The PCR primers were synthesized as shown in Table 1.

Table 1
Primers used for Real-time PCR

Gene	Forward primer sequence (5'-3')	Reverse primer sequence (5'-3')
ALP	AACGTGGCCAAGAACATCATCA	TGTCCATCTCCAGCCGTGTC
BMP-2	CAACACCGTGCTCAGCTTCC	TTCCCACTCATTTCTGAAAGTTCC
COL1	GCCTCCCAGAACATCACCTA	GCAGGGACTTCTTGAGGTTG
OCN	GGTGCAGACCTAGCAGACACCA	AGGTAGCGCCGGAGTCTATTCA
RUNX2	CCATAACGGTCTTCACAAATCCT	TCTGTCTGTGCCTTCTTGGTTC
OSX	AAGGCAGTTGGCAATAGTGG	TGAATGGGCTTCTTCCTCAG
GAPDH	GGCACAGTCAAGGCTGAGAATG	ATGGTGGTGAAGACGCCAGTA

ALP staining

The cell inoculation and culture was the same as in the Real-time PCR assay. After culturing for 7 and 14 days, the cells on the Ti samples were washed with PBS and fixed. ALP was stained with the BCIP/NBT ALP color development kit for 15 min. The samples were washed thoroughly with PBS to acquire the images.

Collagen secretion

The cell inoculation and culture was the same as in the Real-time PCR assay. After culture of 7 and 14 days, the cultures were washed by PBS and fixed by 4% paraformaldehyde. Then the collagen secretion was stained by 0.1wt% Sirius red in saturated picric acid for 18 h. The unbound stain was removed in 0.1 M acetic acid and then the images were collected. To quantitatively assess the collagen secretion, the stain on the samples was eluted in 500 μl destain solution (0.2 M NaOH/methanol 1:1) and the optical density at 540 nm was measured using a spectrophotometer.

ECM mineralized nodule displaying

The cell inoculation and culture was the same as in the Real-time PCR assay. After culturing for 14 and 28 days, the cells were washed twice with PBS and then fixed with 60% isopropanol for 1 min. After rehydrating with distilled water for 2–3 min, the ECM mineralized nodules formed by MSC culture were stained with 1wt% alizarin red for 3 min. After thorough washing with distilled water, the images were taken.

In vivo osseointegration

Implant surgery

The animal experiment was approved by the Animal Research Committee of the Fourth Military Medical University and conducted in accordance with the international standards on animal welfare. Twenty female Sprague Dawley rats, aged 3 months and weighing approximately 250 g, were randomly divided into 5 groups: antimiR–138 group, antimiR-control group, CS group, MAO group and polished Ti (PT) group (n = 8 for each group). The femur model was applied for implantation in this study, and the procedure of the surgery was similar to that described before [39]. Briefly, after anesthesia by pelltobarbitalum natricum, the hind limbs were prepared by shaving and cleaning using ethanol and 10% povidone iodine. Then, an incision was made over the distal side of the knee. Gentle dissection was used to move aside the ligament and patella to expose the intercondylar notch of the distal femur. For placement of the screw implant, dental burs and a surgical motor (OsseoSet 200, Nobel Biocare AB, Gothenburg, Sweden) with a low rotational drill speed (800 rpm) were used to prepare a 2.8 mm cylindrical hole at the intercondylar notch of the femur parallel to the long axis of the bone cooled continuously with sterile saline solution. Implants were inserted into the femoral medullary canal, followed by incision suture. The animals received injection of gentamicin (1 mg/kg) immediately after surgery and for five post-operative days.

Micro-CT evaluation

Specimens (femurs containing implants) were extracted (n = 4 per group) and fixed in 4% paraformaldehyde for 24 h. Then they were scanned by a micro-CT scanner (YXLON International GmbH, Hamburg, Germany). The region of interest (ROI) was defined as 2 mm height from 0.5 μm below the growth plate and 200 μm around the implant surface, and the images were analyzed via VGStudio Max 2.2 (Volume Graphic, Heidelberg, Germany). The bone volume per total volume (BV/TV), the mean trabecular thickness (Tb.Th), the mean trabecular number (Tb.N) and the mean trabecular separation (Tb.Sp) were assessed within the ROI zone.

Van Gieson Staining

After micro-CT scanning, the specimens were dehydrated with graded alcohol, and embedded in methyl methacrylate. Afterwards, thin sections (about 50 μm in thickness) parallel to the long axis of the implants were prepared using a macrocutting and grinding system (SP1600 and SP2600, Leica). Sections were then polished and stained with 1.2% trinitrophenol and 1% acid fuchsin (Van-Gieson staining). Finally, qualitative analysis of bone formation was measured with a standard light microscope (Leica) equipped with a digital image analysis system (Image-Pro Plus software, Media Cybernetics, Silver Spring, USA). Bone-implant contact (BIC) was also determined.

Line-Scanning of the Bone-to-Implant Interface

Line scanning by energy-dispersive X-ray spectroscopy (EDX, Hitachi) was applied for more detailed analysis of the bone-to-implant interface. After being fixed with 4% paraformaldehyde, dehydrated with graded alcohol, and embedded in methyl methacrylate, the bone-to-implant interfaces of the embedded samples were scanned by FE-SEM. The line-profiles of C, O, Ca, P, and Ti elements from the implant side to medullary cavity side were analyzed by EDX.

Statistical analysis

The one-way ANOVA and Turkey post hoc tests were used to determine the level of statistical significance of difference among groups. $p < 0.05$, 0.01 and 0.001 was set to be significant, highly significant and extremely significant, respectively.

Results

Characterization of the CS-antimiR–138/HA PEM functionalized microporous Ti surface Contact angle measurement

During the growth of the CS-antimiR–138/HA PEM functionalized microporous Ti surface, we monitored the wettability of each monolayer. As shown in Fig. 1, the naked MAO Ti surface marked as monolayer 0 was hydrophilic with the lowest water contact angle of ~20°. The initial adsorbed APTES and GA layers, named monolayer 1 and 2, respectively, were both less hydrophilic than the naked MAO, showing contact angles of approximately 50° and 35°. After the growth of monolayer 3 on the surface, which was CS, the contact angle decreased. Afterwards, the addition of monolayers displayed alternating decreased and increased contact angles until monolayer 13. Totally, the HA monolayer on the surface produced lower contact angles than the CS-antimiR–138 one.

SEM and fluorescent observation

The morphology of the MAO Ti surfaces before and after PEM functionalization was observed by FE-SEM (Fig. 2). The naked MAO surface has a typical MAO microporous structure (Fig. 2a–c). After the silane-glutaraldehyde coupling process, there was no apparent changing in the structure (Fig. 2d–f). For the CS-miRNA/HA PEM functionalized microporous Ti surface, the CS-miRNA NPs distributed evenly on the microporous structure (Fig. 2g–i). They slightly decreased the diameters of the micropores, even filled some of the smaller micropores up by attaching to the sidewalls of the micropores.

To observe the miRNA loading and release, the Cy3-labeled miRNAs were used to fabricate the CS-antimiR–138/HA PEM functionalized microporous Ti surface. It was scanned by the laser scanning confocal microscopy from surface to bottom layer by layer with an interlayer distance of 400 nm (Fig. 3a–i). From the fluorescence images, we can observe that the miRNAs distributed relatively evenly and entered into the pores. Fig. 3a and i show the top and bottom layer of the CS-antimiR–138/HA PEM coating, respectively. Hence, the total thickness of the CS-antimiR–138/HA PEM coating is estimated to be about 3.2 μm. From the middle layers (Fig. 3b–h), we can observe a lot of fluorescence rings, which were formulated by the deposited CS-miRNA NPs on the sidewalls of micropores. To display the miRNA release, the three-dimensional images (Fig. 3j, k) were reconstructed through the software after layer by layer scanning, which display the miRNA amount before and after 7 days of immersion in the culture medium. There are still certain amounts of miRNAs retaining on the surface and the sidewalls of the micropores after 7 days, indicating the good retension of the CS-miRNA NPs to the Ti surface and potential sustained release of the miRNAs.

Quantification of miRNA loading and release of the CS-miRNA/HA PEM functionalized microporous Ti surface

The accumulative loading profiles were calculated (Fig. 4). The accumulated miRNA loading amount increased gradually with the layer number, indicating that the LbL approach can be used to control the miRNA loading amount (Fig. 4a). The miRNAs released steadily from the CS-miRNA/HA PEM functionalized microporous Ti surface without apparent initial burst release (Fig. 4b). In the first 4 days, nearly 50% of the loaded miRNAs was released from the functionalized surface. At 14 days, ~0.8 μg in total was released, which was nearly 100% of the loaded amount.

Transfection efficiency of the CS-miRNA/HA PEM functionalized microporous Ti surface

To vividly observe the internalization of the miRNAs to the cells, the Cy3-labeled antimiR–138 were used to fabricate the functionalized Ti surface, and then MSCs were seeded on it for 24 h of transfection. The miRNAs showed red color, and the cell nucleus and membrane were stained with blue and green colors,

respectively (Fig. 5A). We observed that after 24 h of incubation, the miRNAs mainly located in the cell body and around the nucleus, suggesting successful intake of the CS-miRNA NPs by the cells. Most cells have intracellular miRNAs in them, indicating a high transfection efficiency of the functionalized Ti surface.

To assess the down-regulatory effect of the CS-antimiR–138/HA PEM functionalized microporous Ti surface on the intracellular miR–138 level, the intracellular miR–138 amount was measured by miRNA PCR (Fig. 5B). The miR–138 level in MSCs seeded on the CS-antimiR–138/HA PEM functionalized microporous Ti surface was successfully down-regulated by approximately 70%.

Cell viability and cytotoxicity

Cell viability measured by the CCK–8 assay is shown in Fig. 6a. The cells cultured on the tissue culture plate (blank control), the naked MAO surface, the CS coated MAO surface, and the PEM functionalized microporous Ti surfaces with antimiR–138 or antimiR-control showed similar cell viability, indicating that the CS-antimiR–138/HA PEM functionalized microporous Ti surface possesses good cytocompatibility.

Meanwhile, the LDH released by cells when co-cultured with the samples was evaluated as an indicator of cytotoxicity (Fig. 6b). The cells cultured on the tissue culture plate (blank control), the naked MAO surface, the CS coated MAO surface, and the PEM functionalized microporous Ti surfaces with antimiR–138 or antimiR-control induced similar LDH release from the cells cultured on them, suggesting that the CS-antimiR–138/HA PEM functionalized microporous Ti surface shows no cytotoxicity.

Cell attachment and morphology

The MSC attachment and spreading on the Ti samples were observed by FE-SEM (Fig. 7). Generally, the cells attached well to the microporous structure and showed very similar polygonal cell morphology and similar spreading area on the microporous Ti surface and the PEM functionalized microporous Ti surfaces with antimiR–138 or antimiR-control. Nonetheless, on the CS-antimiR–138/HA PEM functionalized microporous Ti surface, the filopodia extended from the cells seemed to be thicker than those on the other two surfaces. The cellular filopodia on the CS-antimiR–138/HA PEM functionalized microporous Ti surface were found to anchor into the micropores. Such a phenomenon was not observed on the other two control surfaces. Further, there were many granules on the dorsal side of the cells on the CS-antimiR–138/HA PEM functionalized microporous Ti surface, indicating that the cells on the CS-antimiR–138/HA PEM functionalized microporous Ti surface have a more mature secretory phenotype.

Effect of the CS-antimiR–138/HA PEM functionalized microporous Ti surface on osteogenesis in vitro

The expression levels of osteogenesis related genes were assessed by Real-time PCR (Fig. 8). Generally, the CS-antimiR–138/HA PEM functionalized microporous Ti surface induced strikingly higher expression levels of BMP–2, OCN, COL1, ALP, OSX and RUNX2 by MSCs than the CS-antimiR-control/HA PEM functionalized microporous Ti surface, the CS coated surface as well as the naked MAO surface. There was no obvious difference in the expression levels of those genes among the CS-antimiR-control/HA PEM functionalized microporous Ti surface, the CS coated surface as well as the naked MAO surface.

Then the ALP product and collagen secretion after 7 days of culture as well as the ECM mineralization after 14 days of culture were assessed (Fig. 9). The MSCs produced the most amount of ALP on the CS-antimiR–138/HA PEM functionalized microporous Ti surface after 7 days of osteogenic induction (Fig. 9a–d). There was no obvious difference in the induced levels of ALP production among the antimiR-control/HA PEM functionalized microporous Ti surface, the CS coated surface as well as the naked MAO surface.

Collagen secretion was stained via Sirius red and the results are shown in Fig. 9a'–d'. The optical images show that much more intensive collagen was secreted by cells on the CS-antimiR–138/HA PEM functionalized microporous Ti surface, compared to the antimiR-control/HA PEM functionalized microporous Ti surface, the CS coated surface as well as the naked MAO surface. The quantitative results indicate that the collagen amount on the CS-antimiR–138/HA PEM functionalized microporous Ti surface was approximately double that on the naked MAO surface, and triple those on the antimiR-control/HA PEM functionalized microporous Ti surface and the CS coated surface.

Next, the ECM mineralized nodules were stained via alizarin red, and the results are shown in Fig. 9a"–d". The mineralized nodules formed by the MSCs were observed on the optical images after 14 days of culture on all four surfaces, and the CS-antimiR–138/HA PEM functionalized microporous Ti surface generated the most amounts of mineralized nodules. The quantitative results reveal that the CS-antimiR–138/HA PEM functionalized microporous Ti surface induced more mineralized nodules about 2 times those formed on the three control groups.

In Vivo Osseointegration of the CS-antimiR–138/HA PEM functionalized microporous Ti implant

The micro-CT analysis was performed to evaluate the in vivo new bone formation and osseointegration (Fig. 10). The reconstructed 3D stereoscopic pictures of the new bone formation (yellow) around the implants are shown in Fig. 10a. The quantitative evaluation of bone volume ratio (BV/TV) and trabecular architecture are shown in Fig. 10b. The analysis of BV/TV, Tb.Th, Tb.N and Tb.Sp in the ROI revealed that the bone trabecula around the PT surface was the thinnest and sparsest. Compared to the three MAO control groups, the CS-antimiR–138/HA PEM functionalized microporous Ti surface induced obviously more new bone formation (with BV/TV and Tb.N increased by about 40% and Tb.Sp decreased by about half ($p < 0.05$)).

To evaluate the tissue healing progress around the implants, we performed histological analysis on the bone-to-implant interface by Van-Gieson staining. New bone (red) was formed around the implants in all groups 4 weeks after implantation (Fig. 11a). Compared to the PT implant that generated thin and discontinuous new bone on it, the CS-antimiR-control/HA PEM functionalized microporous Ti implant, the CS coated implant and the naked MAO implant induced more bone formation. The CS-antimiR–138/HA PEM functionalized microporous Ti implant generated the largest bone volume and the best bone continuity around the implant surface. Quantitative measurement of bone-to-implant contact (BIC) (Fig. 11b) shows a similar trend. The percent of bone-to-implant contact increased from about 38% on the PT implant to about 85% on the CS-antimiR–138/HA PEM functionalized microporous Ti implant.

The cross-section of the bone-to-implant interface was inspected by FE-SEM (Fig. 12a). The distribution of elements including C, O, P, Ca, and Ti across the interface were analyzed by EDX line scanning (Fig. 12b). The thickness of new bone rich in Ca and P was measured. The antimiR–138 PEM functionalized microporous Ti surface induced the thickest new bone. The thickness of new bone was about 18, 25, 27, 27, and 50 μm for the PT implant, the naked MAO implant, the CS coated MAO implant, the antimiR-control PEM functionalized microporous Ti implant as well as the CS-antimiR–138/HA PEM functionalized microporous Ti implant, respectively.

Discussion

The implant with quicker and tighter osseointegration is a constant requirement from the clinic. Loading the implant surface with therapeutic oligonucleotide is a promising approach for accelerated tissue healing/integration [15, 40–42]. Song et al. had created a siRNA biofunctionalized implant with titania nanotube array coating by cathodic electrodeposition of a CS-siRNA complex [43]. Previously, we have conducted the proof-of-concept studies to fabricate antimiR–138 lipoplexes functionalized Ti implant via lyophilization [22], which demonstrate the feasibility of the miRNA functionalization of Ti implant. However, a more biocompatible carrier instead of liposomes shall be used to avoid cytotoxicity and a sustainable effect shall be obtained by controlling the loading and delivering kinetics of antimiR–138.

In this study, multilayers of CS and HA fabricated by LbL self-assembly technique was used to load miRNA on the Ti implant surface to realize a larger miRNA loading amount and meanwhile a long-lasting release. This technique is based on the alternate adsorption of polyanions and polycations via electrostatic interaction on a charged substrate, and has been widely used for the controlled release of biological molecules [44–46]. To combine the LbL films with the MAO Ti surface firmly, the silane reaction is utilized as the rigid covalent bond could provide firm chemical crosslinking connection between the MAO surface and chitosan. UV irradiation can produce abundant hydroxyl groups on the MAO surface, which could perfectly combine with the ethoxy groups of APTES [38]. The terminal amine group can then be utilized for reaction with the aldehyde groups of glutaraldehyde, which is commonly applied to cross-link with biomolecules [47, 48]. Then, chitosan can be conjugated with a stable covalent bonding onto the MAO Ti surface via the APTES-GA layer, which guarantees stability of the whole self-assembled multilayers on the Ti surface. Furthermore, due to the hydrophobic and positive charge,

chitosan was used as the superficial layer to promote protein adsorption and cell adhesion [49]. The FE-SEM pictures clearly reveal that the MAO treatment formulates a microporous structure topography with potential higher loading capacity [22]. The following silane reaction and PEM formulated a homogeneous coating on the surface without affecting the original MAO microtopography. Using the laser scanning confocal microscopy, it was disclosed that the CS-miRNA complexes indeed entered deeply into the micropores and adhered to the inner sidewalls. The contact angle results again demonstrate that the self-assembly multilayers of chitosan and HA was successfully introduced onto the MAO Ti surface [50, 51].

The miRNA loading profile was analyzed by the fluorescence intensity measurement, which is supposed to be the most sensitive method for RNA quantification [52]. The cumulative loading amount of miRNA increased with the number of layers in a linear relation. The in vitro miRNA release profile had a linear faster release phase in the first 4 days, followed by a slower release phase. The long-lasting release kinetics observed could be attributed to the electrostatic interaction between the negatively and positively charged polymers in PEM [28, 53, 54]. Furthermore, the MAO micropores can protect the nanoparticles against prematurely releasing due to increased contact area and reduced shear force, contributing to the long-lasting release. Taken together, a long-lasting miRNA release of over 2 weeks was observed from the PEM functionalized MAO Ti surface.

Then the miRNA cellular uptake and the transfection efficiency of the CS-antimiR–138/HA PEM functionalized microporous Ti surface were assessed. After cell plating on CS-antimiR–138/HA PEM functionalized microporous Ti surface and transfection of 24 h, there were abundant miRNAs entering into the cells, indicating a high transfection efficiency. This is further verified by the miRNA-PCR. The intracellular target miRNA level was successfully downregulated by approximately 70%. The high transfection efficiency is expected to be related to the microporous Ti surface and the miRNAs retained in the micropores, which leads to localized concentration of miRNA. The direct cellular contact to localized availability of nucleic acids results in improved transfection efficiency [55–57]. This effect is known as the substrate-mediated gene delivery [55, 58, 59].

Good cytocompatibility without cytotoxicity or impairment on cell functions is an elementary requirement for the clinical application of the biofunctionalized implant. Our data demonstrate that the CS-antimiR–138/HA PEM functionalized microporous Ti surface satisfy this requirement. This shall be attributed to the biocompatible nature of CS and HA and APTES/GA functional groups in the PEM. Nolte et al. found very low toxicity of HA/CS coatings [60]. Kuddannaya et al. found that poly(dimethylsiloxane) surfaces functionalized with APTES+GA+proteins showed enhanced MSC osteogenic induction with no cytotoxicity, and the APTES/GA functional groups was suggested to play a role [47, 61]. Via covalent conjugation through APTES+GA, SU–8 surface could be functionalized with collagen type I or fibronectin with biocompatibility for long-term cell culture [62]. The cell attachment and spread influence the ensuing cell functions, which was thus observed by the FE-SEM. The cells displayed very similar cell spreading and presented abundant cell lamellipodia stretching out on the all surfaces, which further illustrates the good cytocompatibility of the CS-antimiR–138/HA PEM functionalized microporous Ti surface. Nonetheless, the CS-antimiR–138/HA PEM functionalized MAO Ti surface induced thicker filopodia and

their anchoring into the micropores, which may lead to more rigid osseointegration. A more mature secretory cell phenotype was observed on the CS-antimiR–138/HA PEM functionalized MAO Ti surface, which is likely due to the inhibition of intracellular miR–138 function by antimiR–138 to promote osteogenic differentiation of MSCs [47].

A proper miRNA is pivotal for achieving satisfactory osteogenic activity for the PEM functionalized implant surface. miR–138 is an important regulator for development of the osteoblast phenotype [18, 22, 63]. It has been reported that miR–138 inhibits osteogenic differentiation of MSCs in vitro and formation of bone in vivo. On the other hand, by inhibiting the focal adhesion kinase signaling pathway, antimiR–138 can promote expression of osteoblast-specific genes, ALP activity, ECM mineralization of MSCs and enhance in vivo ectopic bone formation, suggesting that antimiR–138 is a good therapeutic molecular for enhancing osteogenic [18]. Yan et al. also confirmed that antimiR–138 delivery increased the phosphorylation of ERK1/2 and then increased the osteogenesis related genes in the antimiR–138 transfected MSCs [64]. Tsukamoto et al. found that inhibition of miR–138 with an LNA-modified anti-miR–138 oligonucleotide enhanced osteogenic differentiation of MSCs in vitro [65]. In addition, our previous data also demonstrated the efficiency of antimiR–138 in promoting osteogenic differentiation in vitro [22]. The osteogenesis inducing capacity of the antimiR–138 functionalized microporous coatings in vitro and in vivo is consequently assessed. Excitingly, antimiR–138 resulted in enhanced osteogenic activity in vitro and excellent bone formation in vivo, in accordance with these previous reports.

Conclusions

In this study, we have developed a novel CS-antimiR–138/HA PEM functionalized microporous Ti implant via LbL and silane-glutaraldehyde coupling. It exhibits sustained release of CS-antimiR–138, which can be taken up efficiently by the cells without inducing apparent cytotoxicity. It obviously enhances the in vitro osteogenic differentiation of MSCs and dramatically enhanced in vivo osseointegration, thus being very promising to expedite clinical implant osseointegration.

Declarations

Authors' contributions

KMW and MYL performed in vitro study. KMW and NL performed in vivo study. MYL and NL analyzed the data. LZ and FHM offered help for the analysis of experimental data. KMW, MYL and NL drafted the main part of the manuscript, contributed equally to this work and should be considered as co-first authors. YMZ, LZZ, and ML designed and planned the experiments. KMW and LZZ wrote the manuscript. All authors provided input in the interpretation of results. All authors read and approved the final manuscript.

Acknowledgements

Not applicable.

Competing interests

The authors declare that they have no competing interests.

Availability of data and materials

All data generated or analyzed during this study are included in this published article.

Ethics approval and consent to participate

All animal experiments of this study were carried out at Experimental Animal Center, Fourth Military Medical University, and were approved by Experimental Animal Ethics Committee of the Fourth Military Medical University.

Funding

This study was granted by National Natural Science Foundation of China (grant nos.31500776 and 31570954). Indigenous Innovation Program of Qingdao Municipal Science and Technology Commission (15–9–1–23-jch).

References

1. *Buser D, Sennerby L, De Bruyn H. Modern implant dentistry based on osseointegration: 50 years of progress, current trends and open questions. Periodontol 2000. 2017; 73:7-21.*
2. *Civantos A, Martínez-Campos E, Ramos V, Elvira C, Gallardo A, Abarrategi A. Titanium Coatings and Surface Modifications: Toward Clinically Useful Bioactive Implants. ACS Biomater Sci Eng. 2017; 3:1245-61.*
3. *Buser D, Broggini N, Wieland M, Schenk RK, Denzer AJ, Cochran DL, Hoffmann B, Lussi A, Steinemann SG. Enhanced bone apposition to a chemically modified SLA titanium surface. J Dent Res. 2004; 83:529-33.*
4. *Park JW, Jang JH, Lee CS, Hanawa T. Osteoconductivity of hydrophilic microstructured titanium implants with phosphate ion chemistry. Acta Biomater. 2009; 5:2311-21.*
5. *Iwata N, Nozaki K, Horiuchi N, Yamashita K, Tsutsumi Y, Miura H, Nagai A. Effects of controlled micro-/nanosurfaces on osteoblast proliferation. J Biomed Mater Res A. 2017; 105:2589-96.*
6. *Rupp F, Gittens RA, Scheideler L, Marmur A, Boyan BD, Schwartz Z, Geis-Gerstorfer J. A review on the wettability of dental implant surfaces I: theoretical and experimental aspects. Acta Biomater. 2014; 10:2894-906.*

7. *Yu Y, Jin G, Xue Y, Wang D, Liu X, Sun J. Multifunctions of dual Zn/Mg ion co-implanted titanium on osteogenesis, angiogenesis and bacteria inhibition for dental implants. Acta Biomater. 2017; 49:590-603.*
8. *Lee S, Chang YY, Lee J, Madhurakkat Perikamana SK, Kim EM, Jung YH, Yun JH, Shin H. Surface engineering of titanium alloy using metal-polyphenol network coating with magnesium ions for improved osseointegration. Biomater Sci. 2020.*
9. *Kilian KA, Bugarija B, Lahn BT, Mrksich M. Geometric cues for directing the differentiation of mesenchymal stem cells. Proc Natl Acad Sci U S A. 2010; 107:4872-7.*
10. *Jurczak P, Witkowska J, Rodziewicz-Motowidlo S, Lach S. Proteins, peptides and peptidomimetics as active agents in implant surface functionalization. Adv Colloid Interface Sci. 2020; 276:102083.*
11. *Heller M, Kumar VV, Pabst A, Brieger J, Al-Nawas B, Kämmerer PW. Osseous response on linear and cyclic RGD-peptides immobilized on titanium surfaces in vitro and in vivo. J Biomed Mater Res A. 2018; 106:419-27.*
12. *Parfenova LV, Lukina ES, Galimshina ZR, Gil'fanova GU, Mukaeva VR, Farrakhov RG, Danilko KV, Dyakonov GS, Parfenov EV. Biocompatible Organic Coatings Based on Bisphosphonic Acid RGD-Derivatives for PEO-Modified Titanium Implants. Molecules. 2020; 25.*
13. *Croes M, Akhavan B, Sharifahmadian O, Fan H, Mertens R, Tan RP, Chunara A, Fadzil AA, Wise SG, Kruyt MC et al. A multifaceted biomimetic interface to improve the longevity of orthopedic implants. Acta Biomater. 2020.*
14. *Kammerer PW, Pabst AM, Dau M, Staedt H, Al-Nawas B, Heller M. Immobilization of BMP-2, BMP-7 and alendronic acid on titanium surfaces: Adhesion, proliferation and differentiation of bone marrow-derived stem cells. J Biomed Mater Res A. 2020; 108:212-20.*
15. *Song W, Yang C, Svend Le DQ, Zhang Y, Kjems J. Calcium-MicroRNA Complex-Functionalized Nanotubular Implant Surface for Highly Efficient Transfection and Enhanced Osteogenesis of Mesenchymal Stem Cells. ACS Appl Mat Interfaces. 2018; 10:7756-64.*
16. *Sakurai T, Yoshinari M, Toyama T, Hayakawa T, Ohkubo C. Effects of a multilayered DNA/protamine coating on titanium implants on bone responses. J Biomed Mater Res A. 2016; 104:1500-9.*
17. *Carthew RW, Sontheimer EJ. Origins and Mechanisms of miRNAs and siRNAs. Cell. 2009; 136:642-55.*
18. *Eskildsen T, Taipaleenmaki H, Stenvang J, Abdallah BM, Ditzel N, Nossent AY, Bak M, Kauppinen S, Kassem M. MicroRNA-138 regulates osteogenic differentiation of human stromal (mesenchymal) stem cells in vivo. Proc Natl Acad Sci U S A. 2011; 108:6139-44.*
19. *Xu T, Luo Y, Wang J, Zhang N, Gu C, Li L, Qian D, Cai W, Fan J, Yin G. Exosomal miRNA-128-3p from mesenchymal stem cells of aged rats regulates osteogenesis and bone fracture healing by targeting Smad5. J Nanobiotechnology. 2020; 18:47.*
20. *Zeng HC, Bae Y, Dawson BC, Chen Y, Bertin T, Munivez E, Campeau PM, Tao J, Chen R, Lee BH. MicroRNA miR-23a cluster promotes osteocyte differentiation by regulating TGF-beta signalling in osteoblasts. Nat Commun. 2017; 8:15000.*

21. *Elsafadi M, Manikandan M, Alajez NM, Hamam R, Dawud RA, Aldahmash A, Iqbal Z, Alfayez M, Kassem M, Mahmood A. MicroRNA-4739 regulates osteogenic and adipocytic differentiation of immortalized human bone marrow stromal cells via targeting LRP3. Stem Cell Res. 2017; 20:94-104.*
22. *Wu K, Song W, Zhao L, Liu M, Yan J, Andersen MO, Kjems J, Gao S, Zhang Y. MicroRNA functionalized microporous titanium oxide surface by lyophilization with enhanced osteogenic activity. ACS Appl Mat Interfaces. 2013; 5:2733-44.*
23. *Baghdan E, Pinnapireddy SR, Strehlow B, Engelhardt KH, Schafer J, Bakowsky U. Lipid coated chitosan-DNA nanoparticles for enhanced gene delivery. Int J Pharm. 2018; 535:473-9.*
24. *Cupino TL, Watson BA, Cupino AC, Oda K, Ghamsary MG, Soriano S, Kirsch WM. Stability and bioactivity of chitosan as a transfection agent in primary human cell cultures: A case for chitosan-only controls. Carbohydr Polym. 2018; 180:376-84.*
25. *Nguyen MA, Wyatt H, Susser L, Geoffrion M, Rasheed A, Duchez AC, Cottee ML, Afolayan E, Farah E, Kahiel Z et al. Delivery of MicroRNAs by Chitosan Nanoparticles to Functionally Alter Macrophage Cholesterol Efflux in Vitro and in Vivo. ACS Nano. 2019; 13:6491-505.*
26. *Jiang F, Yin F, Lin Y, Xia W, Zhou L, Pan C, Wang N, Shan H, Zhou Z, Yu X. The promotion of bone regeneration through CS/GP-CTH/antagomir-133a/b sustained release system. Nanomedicine. 2020; 24:102116.*
27. *Decher G, Hong JD, Schmitt J, Decher G, Hong JD, Schmitt J. Buildup of ultrathin multilayer films by a self-assembly process: III. Consecutively alternating adsorption of anionic and cationic polyelectrolytes on charged surfaces. Thin Solid Films. 1992; 210–211:831-5.*
28. *Del Mercato LL, Ferraro MM, Baldassarre F, Mancarella S, Greco V, Rinaldi R, Leporatti S. Biological applications of LbL multilayer capsules: from drug delivery to sensing. Adv Colloid Interface Sci. 2014; 207:139-54.*
29. *Ding I, Shendi DM, Rolle MW, Peterson AM. Growth-Factor-Releasing Polyelectrolyte Multilayer Films to Control the Cell Culture Environment. Langmuir. 2018; 34:1178-89.*
30. *Shah NJ, Hyder MN, Quadir MA, Dorval Courchesne NM, Seeherman HJ, Nevins M, Spector M, Hammond PT. Adaptive growth factor delivery from a polyelectrolyte coating promotes synergistic bone tissue repair and reconstruction. Proc Natl Acad Sci U S A. 2014; 111:12847-52.*
31. *Jewell CM, Lynn DM. Multilayered polyelectrolyte assemblies as platforms for the delivery of DNA and other nucleic acid-based therapeutics. Adv Drug Deliv Rev. 2008; 60:979-99.*
32. *Cheng YC, Guo SL, Chung KD, Hu WW. Electrical Field-Assisted Gene Delivery from Polyelectrolyte Multilayers. Polymers (Basel). 2020; 12.*
33. *Hossfeld S, Nolte A, Hartmann H, Recke M, Schaller M, Walker T, Kjems J, Schlosshauer B, Stoll D, Wendel HP et al. Bioactive coronary stent coating based on layer-by-layer technology for siRNA release. Acta Biomater. 2013; 9:6741-52.*
34. *Koenig O, Neumann B, Schlensak C, Wendel HP, Nolte A. Hyaluronic acid/poly(ethylenimine) polyelectrolyte multilayer coatings for siRNA-mediated local gene silencing. PLoS One. 2019; 14:e0212584.*

35. *Renoud P, Toury B, Benayoun S, Attik G, Grosgogeat B. Functionalization of titanium with chitosan via silanation: evaluation of biological and mechanical performances. PLoS One. 2012; 7:e39367.*
36. *Norowski PA, Courtney HS, Babu J, Haggard WO, Bumgardner JD. Chitosan coatings deliver antimicrobials from titanium implants: a preliminary study. Implant Dent. 2011; 20:56-67.*
37. *Lv H, Chen Z, Yang X, Cen L, Zhang X, Gao P. Layer-by-layer self-assembly of minocycline-loaded chitosan/alginate multilayer on titanium substrates to inhibit biofilm formation. J Dent. 2014; 42:1464-72.*
38. *Han Y, Chen D, Sun J, Zhang Y, Xu K. UV-enhanced bioactivity and cell response of micro-arc oxidized titania coatings. Acta Biomater. 2008; 4:1518-29.*
39. *Dang Y, Zhang L, Song W, Chang B, Han T, Zhang Y, Zhao L. In vivo osseointegration of Ti implants with a strontium-containing nanotubular coating. Int J Nanomedicine. 2016; 11:1003-11.*
40. *Zhang L, Zhou Q, Song W, Wu K, Zhang Y, Zhao Y. Dual-Functionalized Graphene Oxide Based siRNA Delivery System for Implant Surface Biomodification with Enhanced Osteogenesis. ACS Appl Mat Interfaces. 2017; 9:34722-35.*
41. *Huang Y, Zheng Y, Xu Y, Li X, Zheng Y, Jia L, Li W. Titanium Surfaces Functionalized with siMIR31HG Promote Osteogenic Differentiation of Bone Marrow Mesenchymal Stem Cells. ACS Biomater Sci Eng. 2018; 4:2986-93.*
42. *Xing H, Wang X, Xiao G, Zhao Z, Zou S, Li M, Richardson JJ, Tardy BL, Xie L, Komasa S et al. Hierarchical assembly of nanostructured coating for siRNA-based dual therapy of bone regeneration and revascularization. Biomaterials. 2020; 235:119784.*
43. *Song W, Zhao L, Fang K, Chang B, Zhang Y. Biofunctionalization of titanium implant with chitosan/siRNA complex through loading-controllable and time-saving cathodic electrodeposition. J Mater Chem B. 2015; 3:8567-76.*
44. *Yang Y, Zhu H, Wang J, Fang Q, Peng Z. Enzymatically Disulfide-Crosslinked Chitosan/Hyaluronic Acid Layer-by-Layer Self-Assembled Microcapsules for Redox-Responsive Controlled Release of Protein. ACS Appl Mat Interfaces. 2018; 10:33493-506.*
45. *Liu G, Li L, Huo D, Li Y, Wu Y, Zeng L, Cheng P, Xing M, Zeng W, Zhu C. A VEGF delivery system targeting MI improves angiogenesis and cardiac function based on the tropism of MSCs and layer-by-layer self-assembly. Biomaterials. 2017; 127:117-31.*
46. *Iqbal MH, Schroder A, Kerdjoudj H, Njel C, Senger B, Ball V, Meyer F, Boulmedais F. Effect of the Buffer on the Buildup and Stability of Tannic Acid/Collagen Multilayer Films Applied as Antibacterial Coatings. ACS Appl Mater Interfaces. 2020.*
47. *Kuddannaya S, Chuah YJ, Lee MH, Menon NV, Kang Y, Zhang Y. Surface chemical modification of poly(dimethylsiloxane) for the enhanced adhesion and proliferation of mesenchymal stem cells. ACS Appl Mat Interfaces. 2013; 5:9777-84.*
48. *Aydin EB, Aydin M, Sezginturk MK. Electrochemical immunosensor based on chitosan/conductive carbon black composite modified disposable ITO electrode: An analytical platform for p53 detection. Biosens Bioelectron. 2018; 121:80-9.*

49. *Bumgardner JD, Wiser R, Elder SH, Jouett R, Yang Y, Ong JL. Contact angle, protein adsorption and osteoblast precursor cell attachment to chitosan coatings bonded to titanium. J Biomater Sci Polym Ed. 2003; 14:1401-9.*
50. *Costa RR, Custodio CA, Arias FJ, Rodriguez-Cabello JC, Mano JF. Layer-by-layer assembly of chitosan and recombinant biopolymers into biomimetic coatings with multiple stimuli-responsive properties. Small. 2011; 7:2640-9.*
51. *Song W, Song X, Yang C, Gao S, Klausen LH, Zhang Y, Dong M, Kjems J. Chitosan/siRNA functionalized titanium surface via a layer-by-layer approach for in vitro sustained gene silencing and osteogenic promotion. Int J Nanomedicine. 2015; 10:2335-46.*
52. *Jones LJ, Yue ST, Cheung CY, Singer VL. RNA quantitation by fluorescence-based solution assay: RiboGreen reagent characterization. Anal Biochem. 1998; 265:368-74.*
53. *Luo J, Cao S, Chen X, Liu S, Tan H, Wu W, Li J. Super long-term glycemic control in diabetic rats by glucose-sensitive LbL films constructed of supramolecular insulin assembly. Biomaterials. 2012; 33:8733-42.*
54. *Wohl BM, Engbersen JF. Responsive layer-by-layer materials for drug delivery. J Control Release. 2012; 158:2-14.*
55. *Jewell CM, Lynn DM. Surface-Mediated Delivery of DNA: Cationic Polymers Take Charge. Curr Opin Colloid Interface Sci. 2008; 13:395-402.*
56. *Lee EJ, Robinson TM, Tabor JJ, Mikos AG, Suh J. Reverse Transduction Can Improve Efficiency of AAV Vectors in Transduction-Resistant Cells. Biotechnol Bioeng. 2018; 115:3042-9.*
57. *Li BC, Chang H, Ren KF, Ji J. Substrate-mediated delivery of gene complex nanoparticles via polydopamine coating for enhancing competitiveness of endothelial cells. Colloids Surf B Biointerfaces. 2016; 147:172-9.*
58. *Holmes CA, Tabrizian M. Substrate-mediated gene delivery from glycol-chitosan/hyaluronic acid polyelectrolyte multilayer films. ACS Appl Mat Interfaces. 2013; 5:524-31.*
59. *Erfle H, Neumann B, Liebel U, Rogers P, Held M, Walter T, Ellenberg J, Pepperkok R. Reverse transfection on cell arrays for high content screening microscopy. Nat Protoc. 2007; 2:392-9.*
60. *Nolte A, Hossfeld S, Schroeppel B, Mueller A, Stoll D, Walker T, Wendel HP, Krastev R. Impact of polyelectrolytes and their corresponding multilayers to human primary endothelial cells. J Biomater Appl. 2013; 28:84-99.*
61. *Chuah YJ, Kuddannaya S, Lee MH, Zhang Y, Kang Y. The effects of poly(dimethylsiloxane) surface silanization on the mesenchymal stem cell fate. Biomater Sci. 2015; 3:383-90.*
62. *Xue P, Bao J, Chuah YJ, Menon NV, Zhang Y, Kang Y. Protein covalently conjugated SU-8 surface for the enhancement of mesenchymal stem cell adhesion and proliferation. Langmuir. 2014; 30:3110-7.*
63. *Yan J, Chang B, Hu X, Cao C, Zhao L, Zhang Y. Titanium implant functionalized with antimiR-138 delivered cell sheet for enhanced peri-implant bone formation and vascularization. Mater Sci Eng C Mater Biol Appl. 2018; 89:52-64.*

64. Yan J, Zhang C, Zhao Y, Cao C, Wu K, Zhao L, Zhang Y. Non-viral oligonucleotide antimiR-138 delivery to mesenchymal stem cell sheets and the effect on osteogenesis. Biomaterials. 2014; 35:7734-49.
65. Tsukamoto S, Løvendorf MB, Park J, Salem KZ, Reagan MR, Manier S, Zavidij O, Rahmat M, Huynh D, Takagi S et al. Inhibition of microRNA-138 enhances bone formation in multiple myeloma bone marrow niche. Leukemia. 2018; 32:1739-50.

Figures

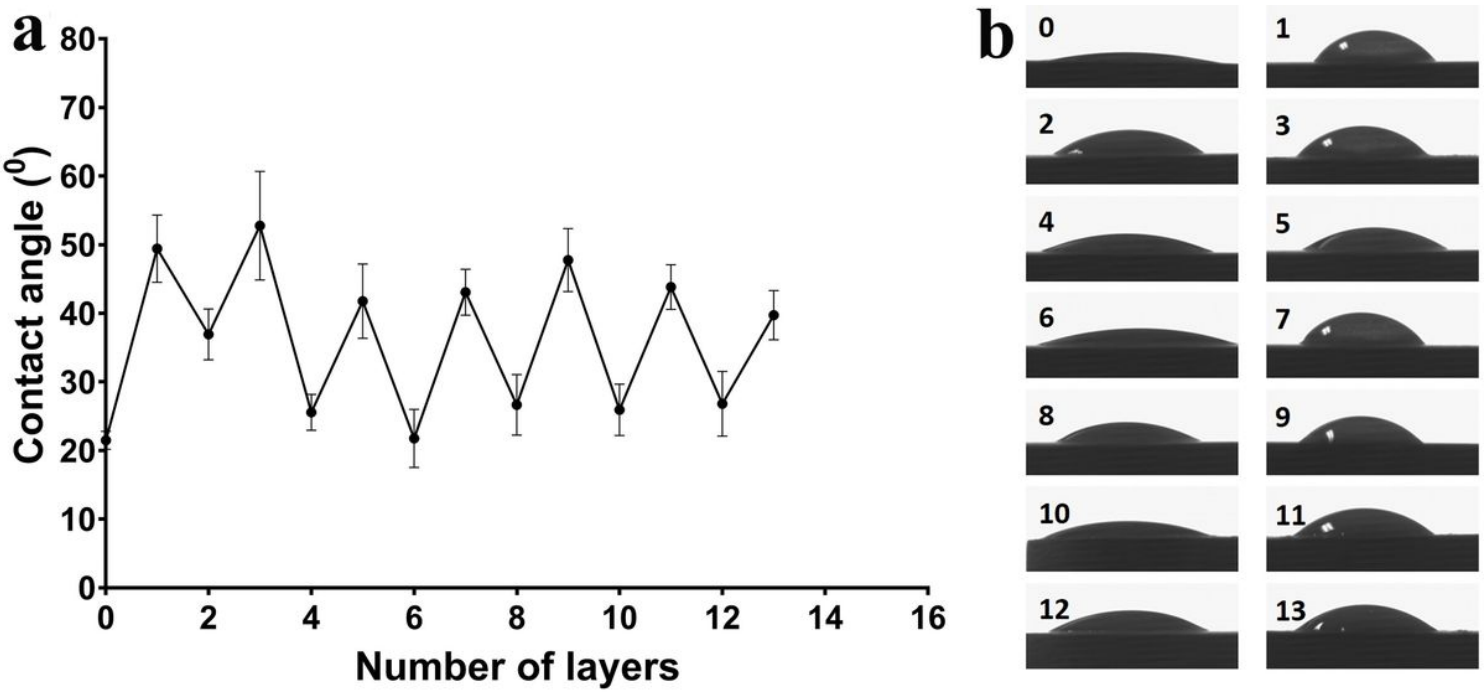

Figure 1

Water contact angles (a) and the lateral views of water drops (b) on the MAO surface after LbL processes

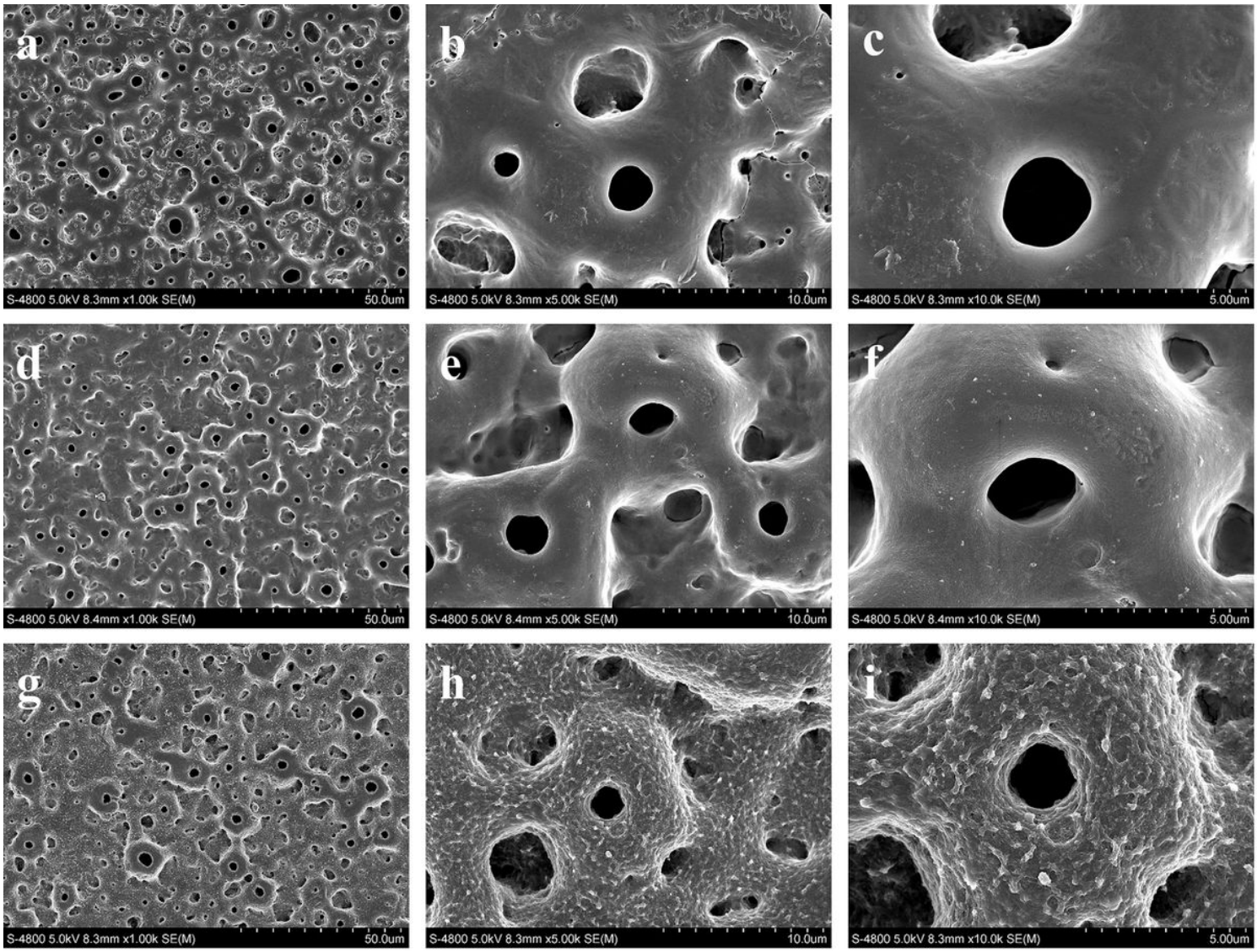

Figure 2

Morphology of the MAO Ti surfaces before and after CS-miRNA/HA PEM functionalized inspected by FE-SEM: (a, b and c) pictures of different magnification for the naked MAO surface; (d, e and f) pictures of silane glutaraldehyde functionalized MAO surface. (g, h and i) pictures of 5 layers for the CS-miRNA/HA PEM functionalized MAO surface.

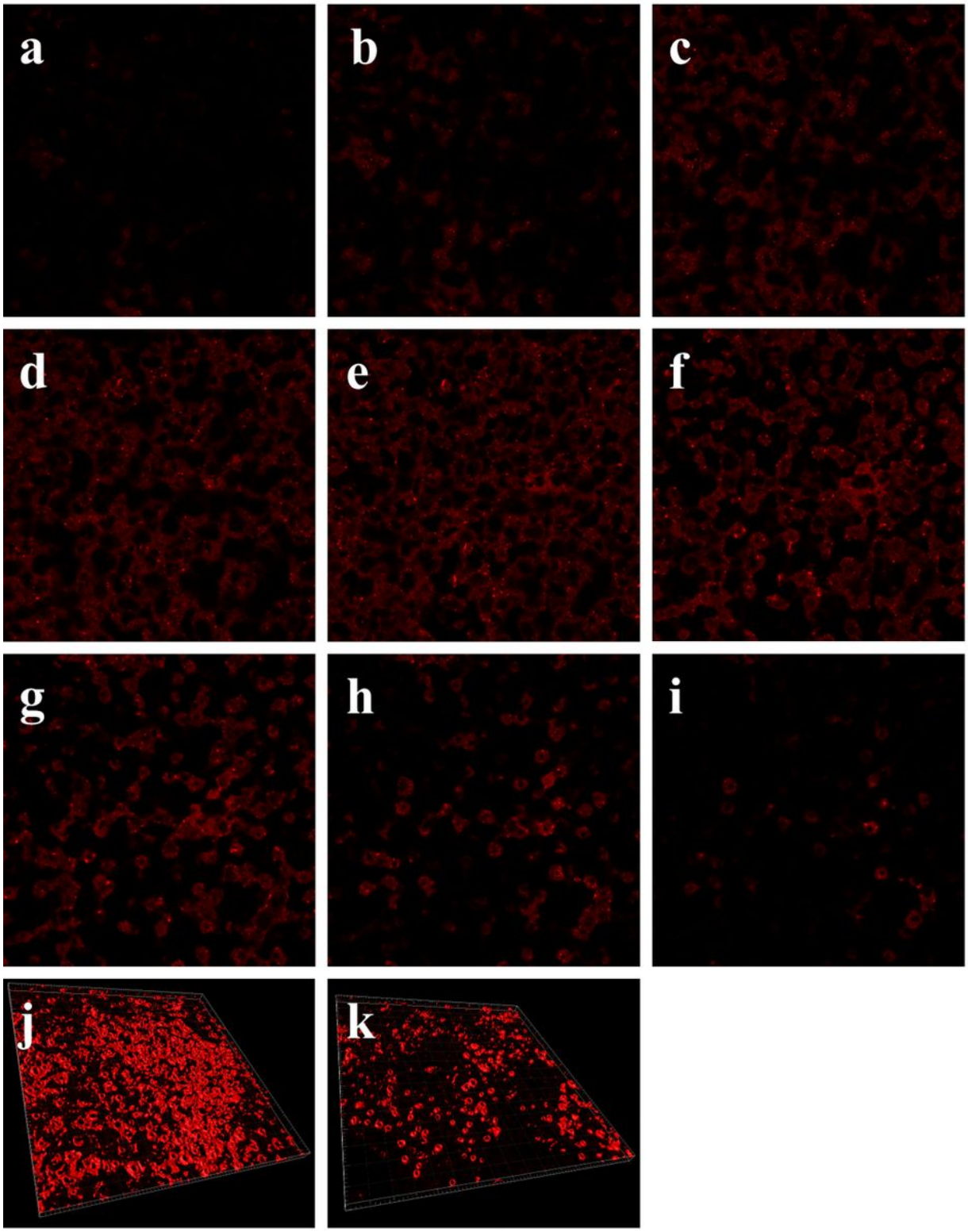

Figure 3

Fluorescence confocal laser scanning microscope of CS-miRNA/HA PEM functionalized MAO surface with Cy3-labeled miRNAs: (a) the top layer starting to display fluorescence and (b-i) the continuing layers from top to down with an interlayer distance of 400 nm. The fluorescence 3-D images of Cy3-labeled miRNAs on the MAO surfaces before (j) and after (k) 7 days of incubation in cell culture medium at 37 °C.

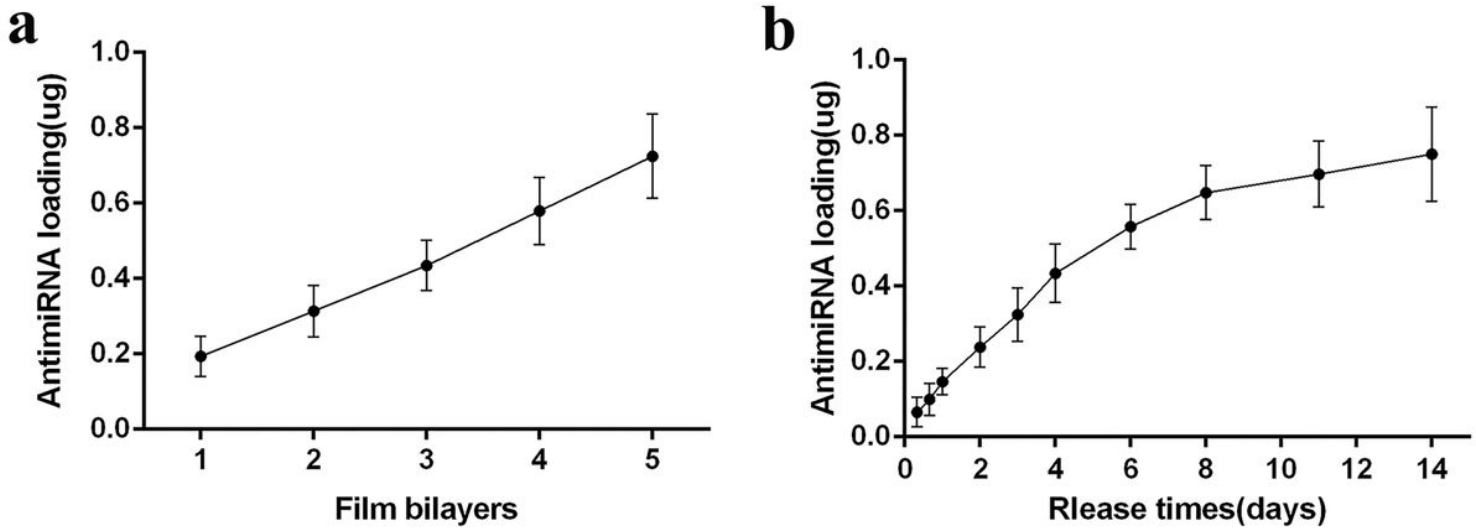

Figure 4

Quantifcation of antimiR-138 on novel CS-antimiR-138/HA PEM functionalized MAO surface. (a) Accumulated antimiR-138 loading amount with increased number of biofunctional layers. (b) Accumulated antimiR-138 release profile from the coated surface.

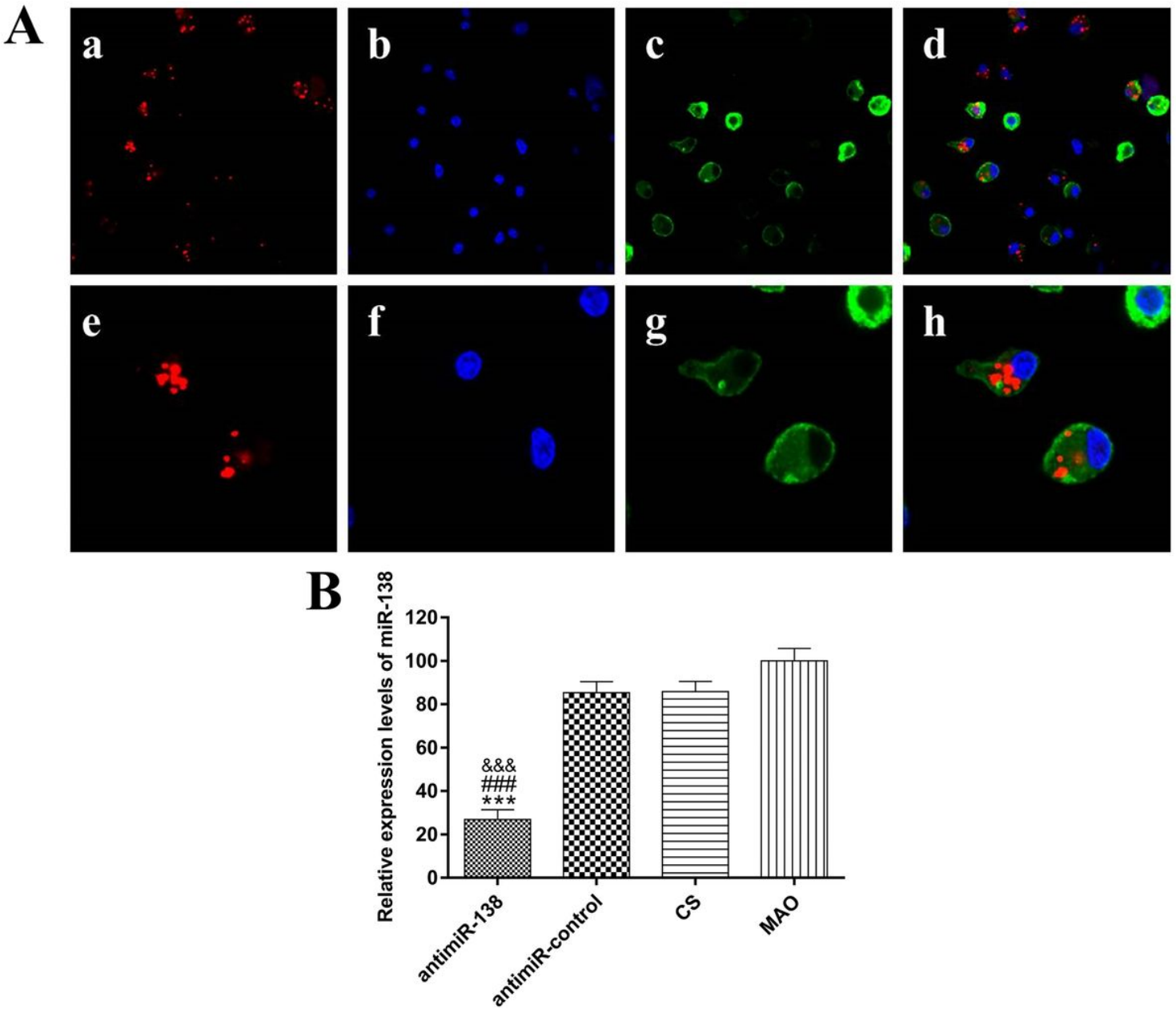

Figure 5

*(A) Fluorescence images of 40× (a, b, c and d) and 120× (e, f, g and h) showing the uptake of miRNAs by cells after 24 h of culture on the CS-miRNA/HA PEM functionalized MAO surface: (a and e) Cy3-labeled miRNAs (red color), (b and f) cell nucleus stained by DAPI (blue color), (c and g) cell membrane stained by DIO (green color), and (d and h) the merged images. (B) Downregulation of microRNA expression by 5 layers miRNA coating. *** p < 0.001 vs the CS-antimiR-control/HA PEM functionalized MAO surface; ### p < 0.001 vs the CS functionalized MAO surface; $$$ p < 0.001 vs the naked MAO surface.*

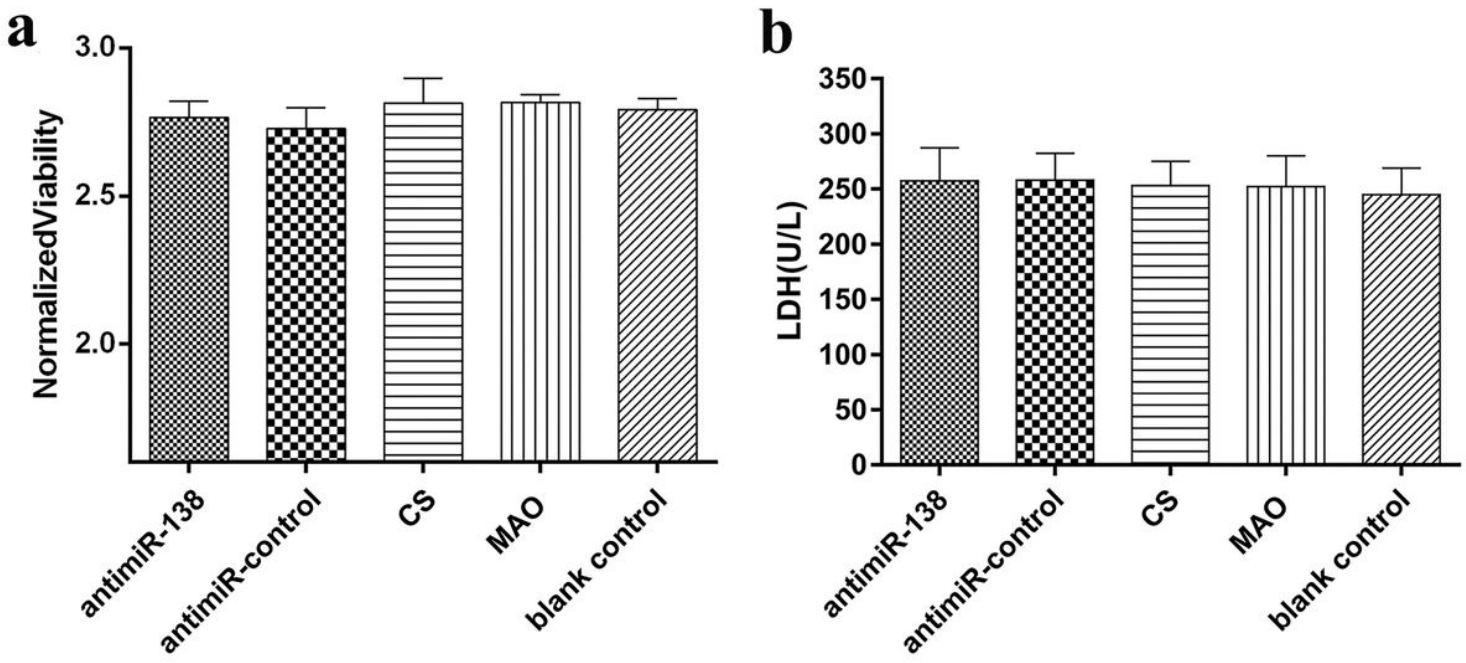

Figure 6

(a) Cell viability measured by CCK-8 at 24 h after transfection and (b) LDH amount released by cells during the first 24 h after transfection.

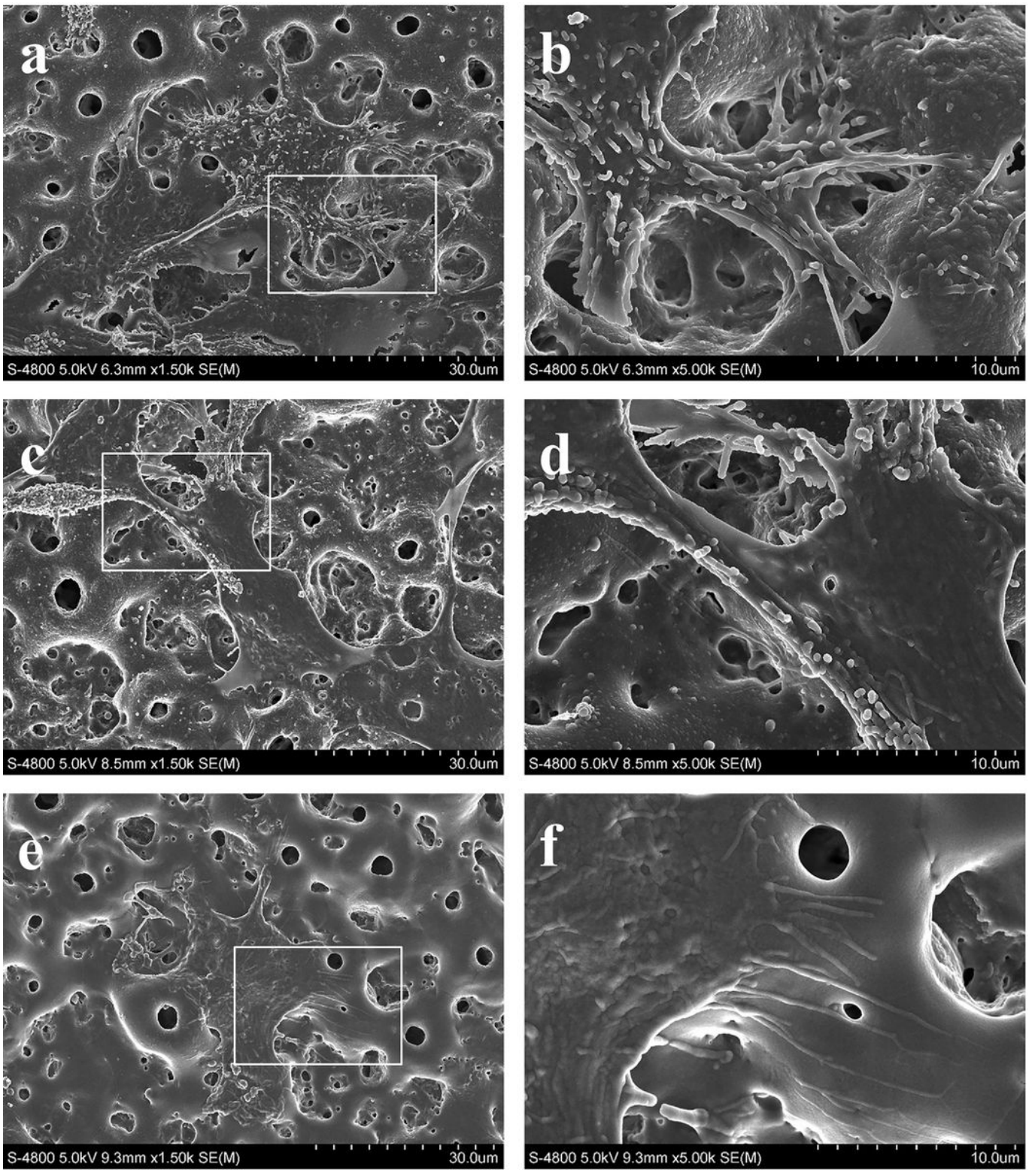

Figure 7

FE-SEM pictures showing the cell morphology after 24 h of incubation on different samples: (a and b) the CS-antimiR-138/HA PEM functionalized MAO surface, (c and d) the antimiR-control PEM functionalized MAO surface and (e and f) the naked MAO surface.

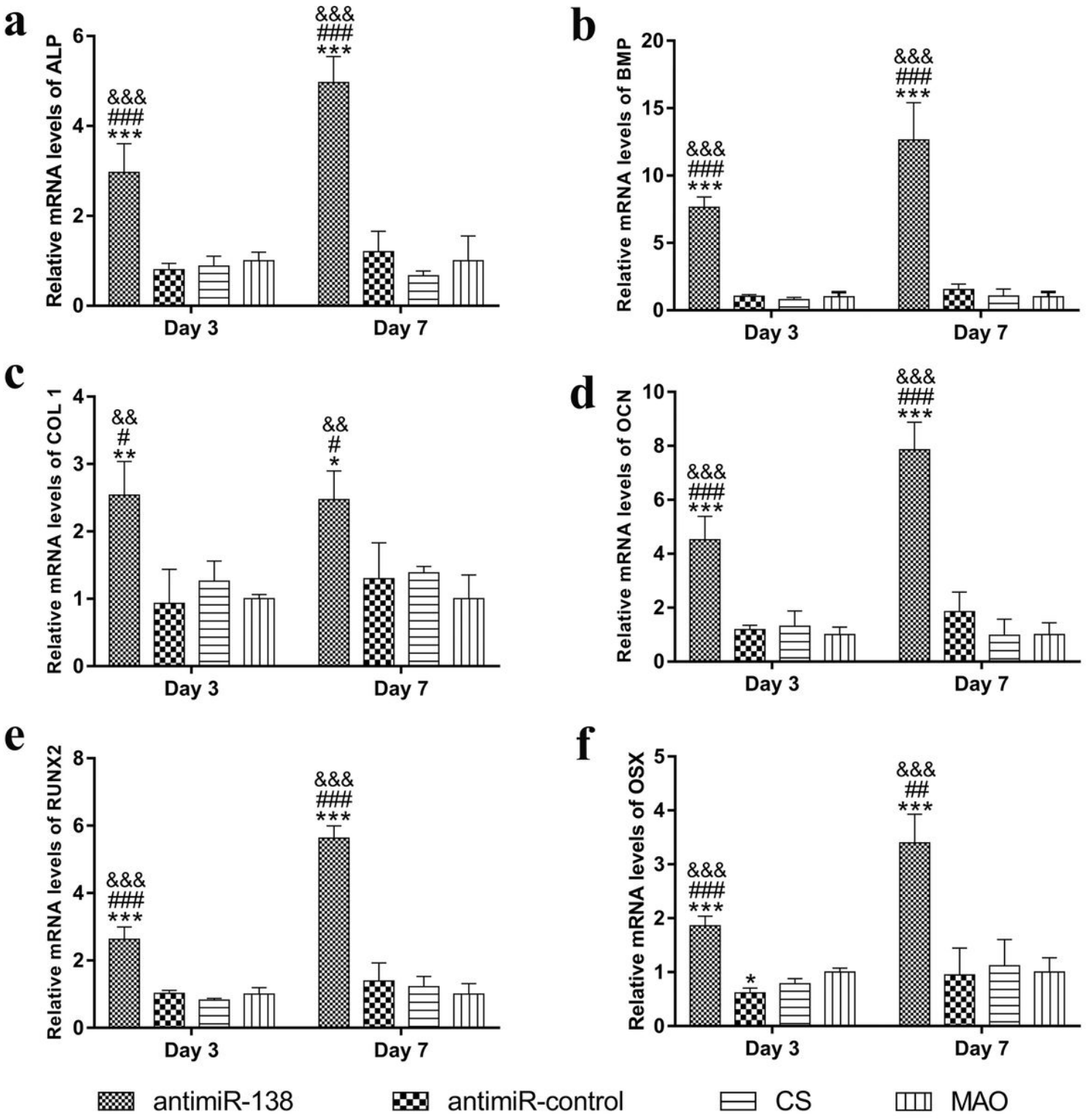

Figure 8

*Relative expression of (a) ALP, (b) BMP, (c) Col1, (d) OCN, (e) OSX and (f) RUNX2 by MSCs cultured on different samples. After culturing in the growth medium for 24 h, the medium was changed to osteogenic medium for further culture of 3 and 7 days. All values are normalized to GAPDH. *, **, *** p <0.05, 0.01 and 0.001 vs the naked MAO surface; #, ##, ### p < 0.05, 0.01 and 0.001 vs the CS functionalized MAO surface; @@, @@@ p < 0.01 and 0.001 vs the CS-antimiR-control/HA PEM functionalized MAO surface.*

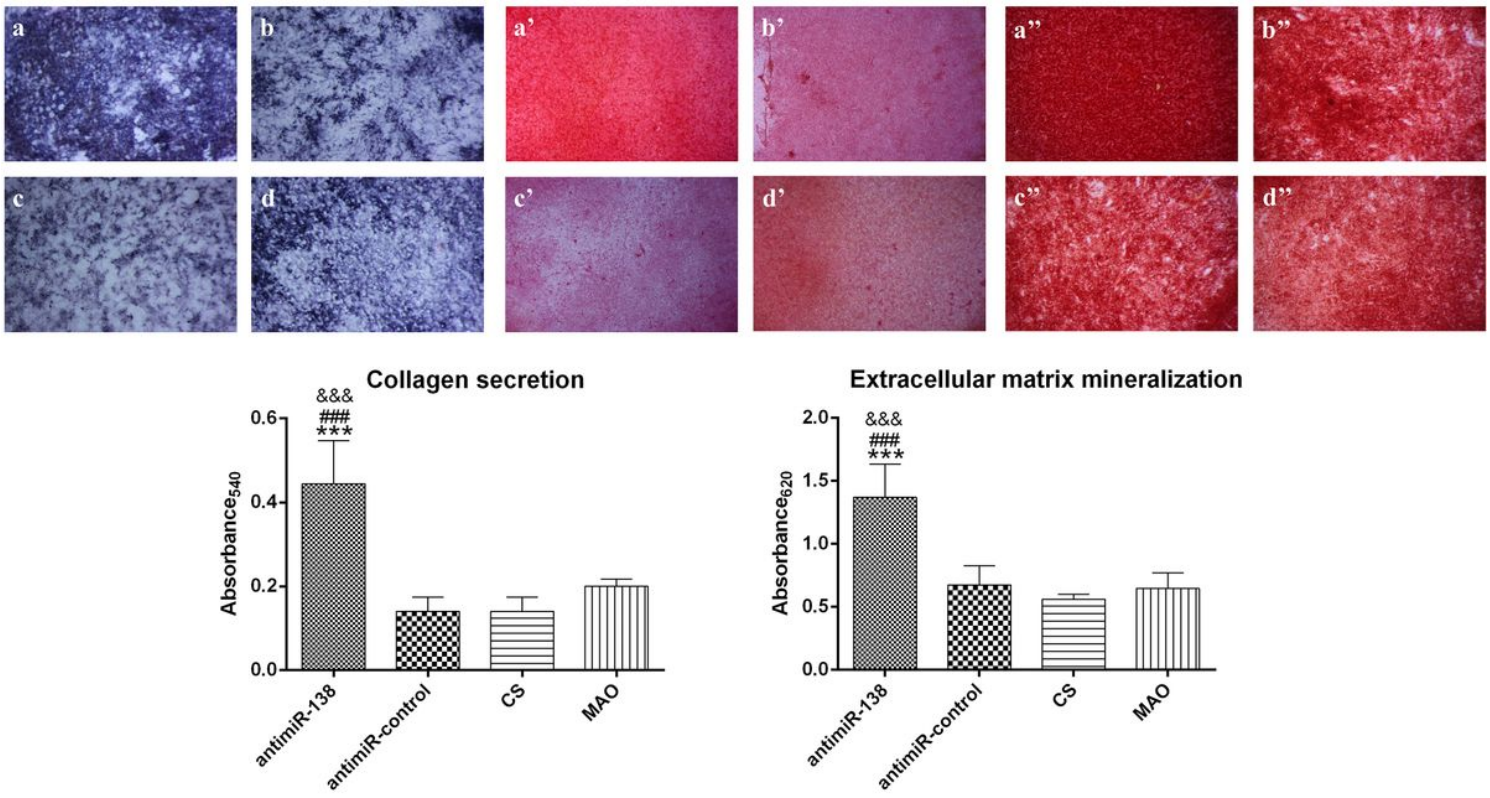

Figure 9

*The ALP product and collagen secretion after 7 days of culture as well as the ECM mineralization after 14 days of culture: (a, a' and a") the CS-antimiR-138/HA PEM functionalized MAO surface, (b, b' and b") the CS-antimiR-control/HA PEM functionalized MAO surface, (c, c' and c") the CS functionalized MAO surface and (d, d' and d") the naked MAO surface. The bottom panel shows the semi-quantitative results. *** p < 0.001 vs the naked MAO surface; ### p < 0.001 vs CS functionalized MAO surface; &&& p < 0.001 vs the CS-antimiR-control/HA PEM functionalized MAO surface.*

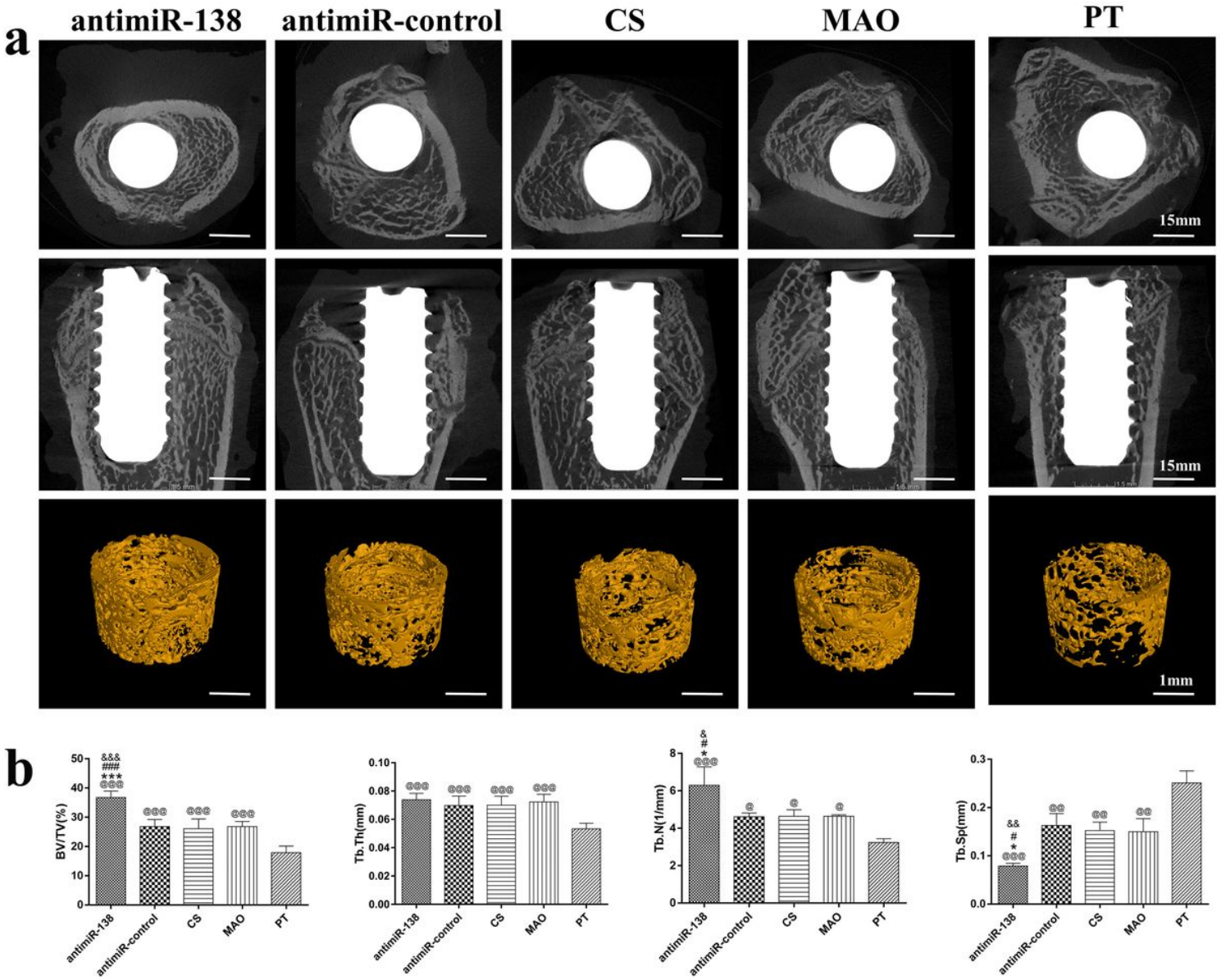

Figure 10

*(a) Transverse and vertical 2-D images and 3-D reconstructed views (ROI, 200 μm from the implant surface) of the Micro-CT analysis to show the new bone formation around the Ti implants at 4 weeks. Scale bar: 15 mm on the 2-D images and 1 mm on the 3-D ones. (b) The bone volume per total volume (BV/TV), the mean trabecular thickness (Tb.Th), the mean trabecular number (Tb.N) and the mean trabecular separation (Tb.Sp) within the ROI zone. @, @@, @@@ p < 0.05, 0.01 and 0.001 vs the PT surface *, *** p <0.05 and 0.001 vs the naked MAO surface; #, ### p < 0.05, and 0.001 vs the CS functionalized MAO surface; &, &&, &&& p < 0.05, 0.01 and 0.001 vs the CS-antimiR-control/HA functionalized MAO surface.*

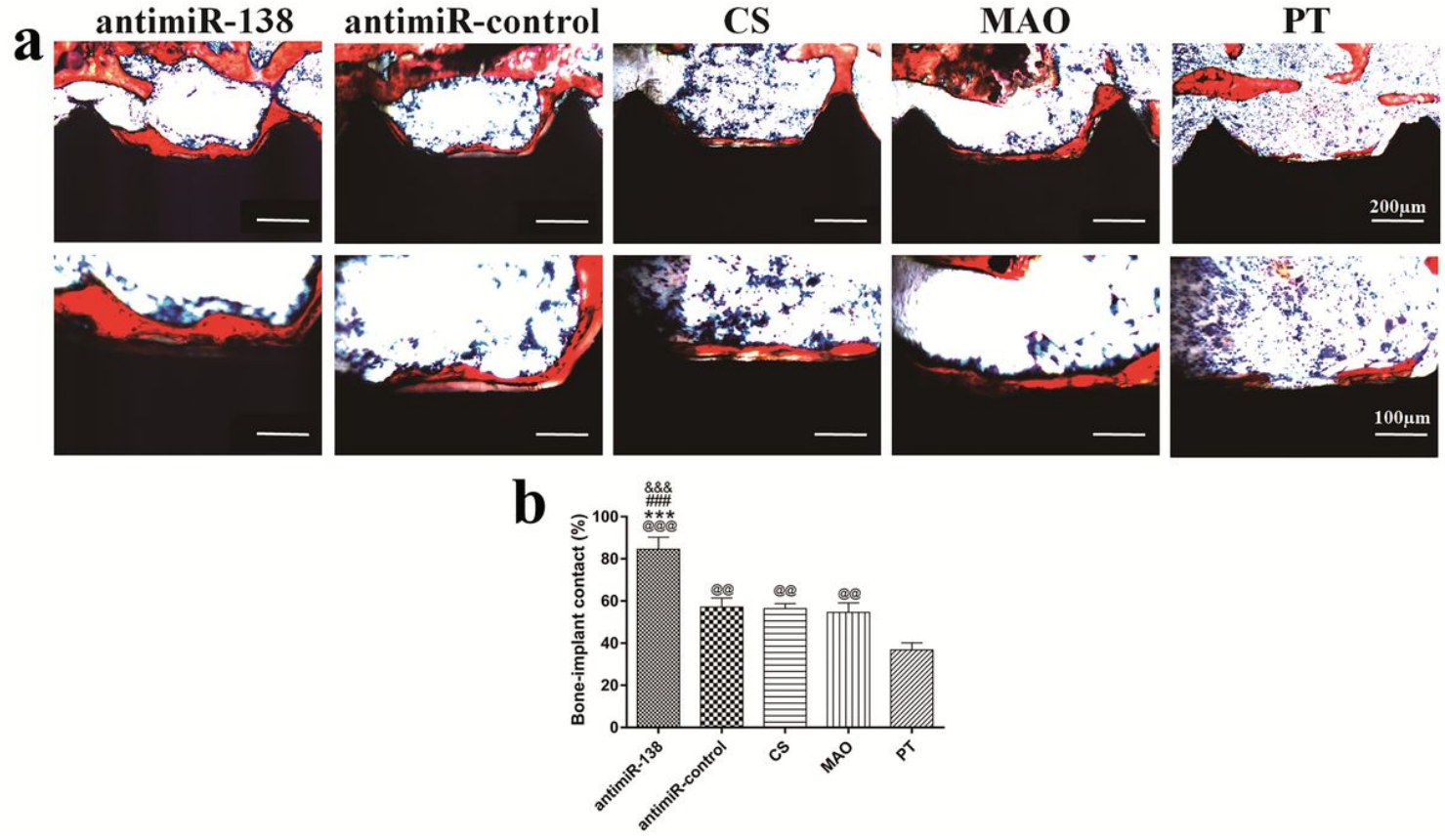

Figure 11

*(a) Histological images of undecalcified sections of new bone formation around the implants at 4 weeks by Van Gieson staining. The bone tissue was stained in red color. Scale bar: 200 μm on the above and 100 μm on the below. (b) Histomorphometric measurement of the Bone-to-implant contact in the ROI. @@, @@@ p < 0.01 and 0.001 vs the PT surface *** p < 0.001 vs the naked MAO surface; ### p < 0.001 vs the CS functionalized MAO surface; &&& p < 0.001 vs CS-antimiR-control/HA functionalized MAO surface.*

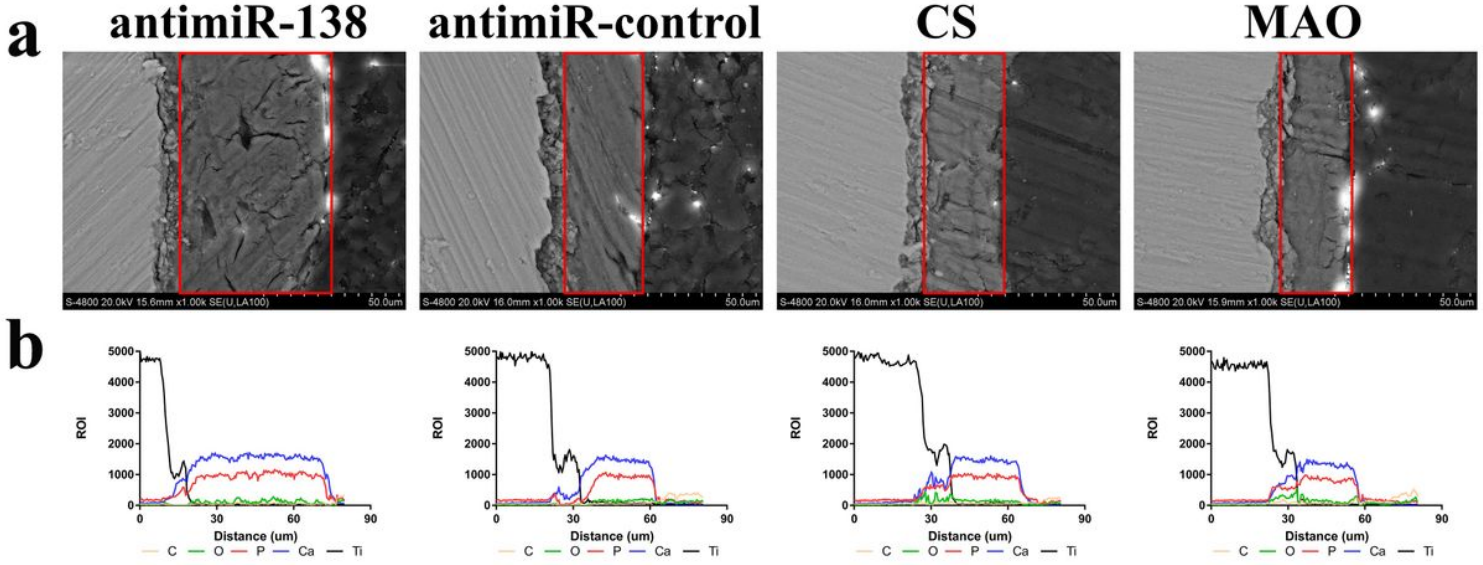

Figure 12

(a) FE-SEM pictures showing the new bone on the bone-to-implant interface of different samples. (b) EDX line scanning of the elements in the direction perpendicular to the bone-to-implant interface. Red frame indicates the new bone area on the implant surface.

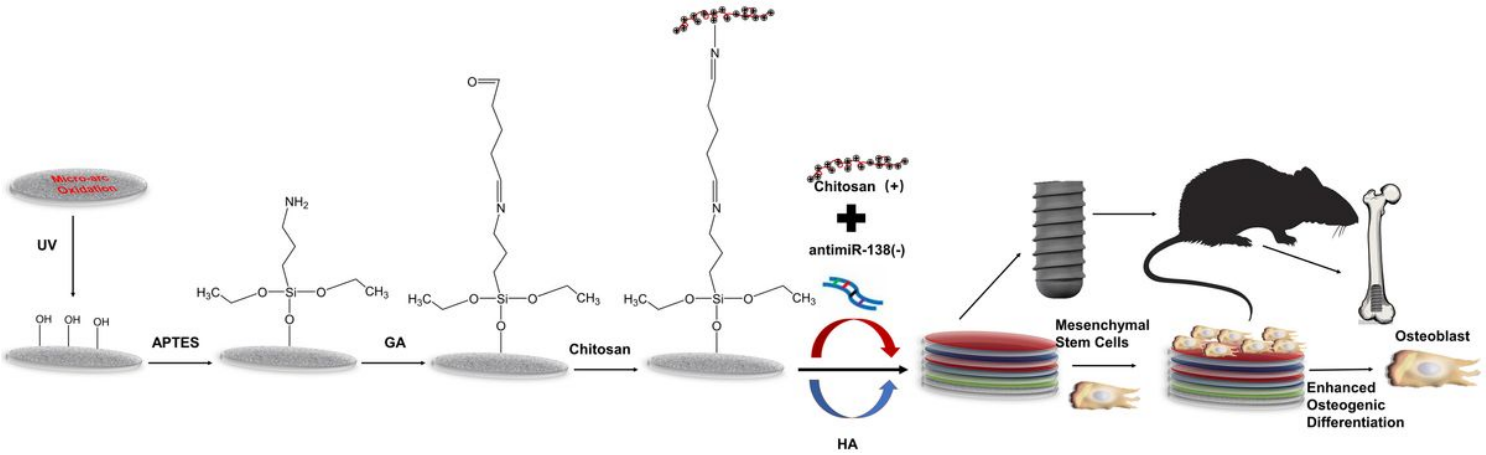

Figure 13

Schematic diagram summarizing the fabrication of the CS-antimiR-138/HA PEM functionalized microporous Ti implant through LbL with enhanced osteogenic activity.